J. Fluid Mech. (2021), *vol*. 915, A136, doi:10.1017/jfm.2021.165

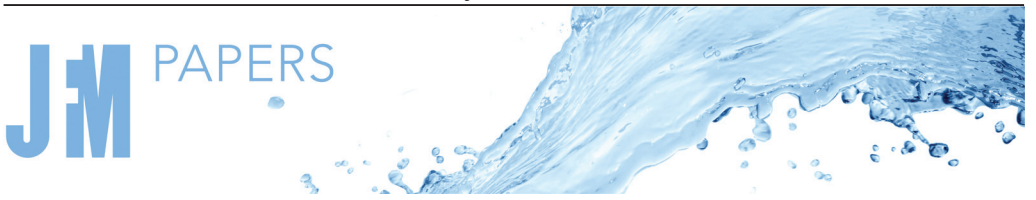

Finite-amplitude steady-state resonant waves in a circular basin

Xiaoyan Yang[1,2], Frederic Dias[3], Zeng Liu[4] and Shijun Liao[2,5,6,†]

[1]Faculty of Maritime and Transportation, Ningbo University, Ningbo 315211, PR China

[2]School of Naval Architecture, Ocean and Civil Engineering, Shanghai Jiao Tong University, Shanghai 200240, PR China

[3]School of Mathematics and Statistics, University College Dublin, Belfield, Dublin 4, Ireland

[4]School of Naval Architecture and Ocean Engineering, Huazhong University of Science and Technology, Wuhan 430074, PR China

[5]State Key Laboratory of Ocean Engineering, Shanghai 200240, PR China

[6]State Key Laboratory of Plateau Ecology and Agriculture, School of Hydraulic and Electric Engineering, Qinghai University, Xining 810018, PR China

(Received 30 March 2020; revised 3 January 2021; accepted 18 February 2021)

The steady-state second-harmonic resonance between the fundamental and the second-harmonic modes for waves in a circular basin is investigated by solving the water-wave equations as a nonlinear boundary-value problem. The resulting waves are called (1,2)-waves. The geometry of the basin allows for both travelling waves (TW) and standing waves (SW). A solution procedure based on a homotopy analysis method (HAM) approach is used. In the HAM framework, the mathematical obstacle due to the singularity corresponding to the resonant-wave component can be overcome by adding the resonant term in the initial guess of the velocity potential. Approximate homotopy-series solutions can be obtained for both (1,2)-TW and (1,2)-SW. Two branches of (1,2)-TW and two branches of (1,2)-SW are found. They bifurcate from the trivial solution. For (1,2)-TW, the HAM-based approach is combined with a Galerkin numerical-method-based approach to follow the branches of nonlinear solutions further. The approximate homotopy-series solutions are used as initial guesses for the Galerkin method. As the nonlinearity increases, an increasing number of wave components are involved in the solution.

Key words: waves/free-surface flows

† Email address for correspondence: sjliao@sjtu.edu.cn

© The Author(s), 2021. Published by Cambridge University Press

https://doi.org/10.1017/jfm.2021.165 Published online by Cambridge University Press

1. Introduction

Resonance is an important phenomenon in the nonlinear interaction of water waves. For gravity waves, the most basic resonance is that of resonant quartets described by Phillips (1960), which involves the interaction of third-order nonlinear terms. Higher-order resonant waves also exist (Hammack & Henderson 1993; Annenkov & Shrira 2006; Liu & Liao 2014). Resonant triads can occur in capillary-gravity waves (Wilton 1915; McGoldrick 1965; Vanden-Broeck 1984; Jones & Toland 1985; Bridges 1990; Dias & Bridges 1990; Chabane & Choi 2019), in interfacial waves (Christodoulides & Dias 2019; Chossat & Dias 1995), or in acoustic-gravity waves (Kadri & Stiassnie 2013; Kadri & Akylas 2016). In addition, the second-harmonic resonance associated with a resonant triad can occur in a circular basin (Mack 1962; Miles 1984). Such resonances can occur in harbours or bays (Bryant 1989; Chossat & Dias 1995), so they have real-world applications.

From the mathematical point of view, much progress was made in the understanding of resonance between two modes by Bridges (1990). He based his study of all space- and time-periodic (m, n)-waves on their symmetries and on the Hamiltonian structure of the water-wave problem. That led him to consider all types of periodic waves, and not travelling waves (TW) or standing waves (SW) in isolation. In the case where two modes resonate, Bridges (1990) showed that in addition to well-known TW and SW other classes of periodic waves, in particular three-mode mixed waves (MW), may exist. The last section of his paper is devoted to the special case of (1,2)-waves. Later, Chossat & Dias (1995), by exploiting in addition the symmetry of time reversibility, showed that the presence of the $O(2)$ symmetry brings non-trivial modifications to the classical $1:2$ resonance.

Waves in a circular basin naturally inherit the $O(2)$ symmetry. Therefore, when considering (1,2)-waves in a circular basin, one expects to find TW, SW and possibly MW. The present paper focuses on TW and SW. We solve the water-wave equations as a nonlinear boundary-value problem. The geometry is a circular basin, with d the ratio of depth to radius. Mack (1962), who studied finite-amplitude symmetric SW in a circular basin, noted that at certain values of d a higher mode at a frequency equal to an integral multiple of the basic frequency has the same order of magnitude as the basic mode (see table 6). Miles (1976) constructed the Lagrangian and Hamiltonian for nonlinear gravity waves in a cylindrical basin and considered resonantly coupled free oscillations. Miles (1976) mentioned that the perturbation solution fails if resonance occurs, but harmonic motions are still possible for special initial conditions, and in general the two modes must be expected to have slowly varying amplitudes and phases. The terminology 'steady-state' is often used to describe solutions with constant amplitudes, as opposed to solutions with slowly varying amplitudes. In the present paper, we only consider steady-state solutions. Miles (1984) gave the critical depths for resonance in a circular basin when the fundamental wave component is the (1,1) mode (see definition in § 2.1). Bryant (1989) obtained multiple families of waves, when searching for steady waves in the neighbourhood of resonances with d as a parameter. The resonance condition reads

$$m(k_{11}\tanh k_{11}d)^{1/2} = (k_{mn}\tanh k_{mn}d)^{1/2}, \tag{1.1}$$

where k_{mn} is defined in § 2.1. The solutions of (1.1) up to $m = 4$ are listed in table 1, which shows the different sets of resonant wave components associated with each of the ratios of depth to radius. The second-harmonic resonance studied in the present paper is obtained when $m = n = 2$.

The stability of (1,2)-waves has been studied by various authors. Bryant (1989) pointed out that steady waves with significant resonant wave components are linearly unstable. Chossat & Dias (1995) considered the slow-time evolution of the amplitudes

https://doi.org/10.1017/jfm.2021.165 Published online by Cambridge University Press

m	n	d
2	2	0.831377
3	2	0.278971
3	3	0.455047
3	4	0.747753
4	2	0.158247
4	3	0.249080
4	4	0.329579
4	5	0.422613
4	6	0.541608
4	7	0.721051
4	8	1.204065

Table 1. Ratios of depth to radius d satisfying the linear resonance relation.

of weakly nonlinear (1,2)-waves. The following statement can be found in Chossat & Dias (1995): 'The analysis shows that the presence of the $\boldsymbol{O}(2)$ symmetry brings non-trivial modifications to the classical 1 : 2 resonance. For example, the persistence of the well-known one-parameter family of homoclinic orbits to "pure-mode" TW is no longer obvious'. The bifurcation analysis performed in the paper of Chossat & Dias (1995) is generic and therefore applies to the steady-state (1,2)-waves we compute in the present paper. However, none of the above studies focuses on the computation of finite-amplitude steady-state waves at exact resonance in a circular basin.

In steady-state (1,2)-waves, the amplitudes of the fundamental wave component and the second harmonic component are of the same order. In the literature, a number of different terminologies are used to describe similar waves: '2-mode mixed TW' in Chossat & Dias (1995), 'mixed type' in Jones & Toland (1985), Wilton ripples in Wilton (1915), McGoldrick (1965), Christodoulides & Dias (1994) and Chabane & Choi (2019).

In recent years, using the homotopy analysis method (HAM) (Liao 1992, 2003, 2010, 2011*a*; Van Gorder & Vajravelu 2008; Vajravelu & Van Gorder 2012; Zhong & Liao 2017, 2018*a*,*b*), Liao (2011*b*) found multiple steady-state resonant gravity waves in deep water as solutions to the water-wave equations. The success in obtaining steady-state resonant wave solutions is attributed to the following advantages of HAM in solving nonlinear problems. First, the HAM provides great freedom to choose the initial guess. When resonance occurs, only the resonant term needs to be added in the initial guess, and the secular term thus generated can be successfully avoided. Additionally, a reasonable selection of the auxiliary linear operator can eliminate singularities with zero denominators in homotopy-series solutions. Furthermore, as opposed to other analytic approximation methods, the HAM can guarantee the convergence of the solution series with the choice of a proper value of the so-called convergence-control parameter c_0. After Liao's work, Xu *et al.* (2012) successfully obtained convergent solutions of steady-state resonant gravity waves, consisting of two progressive primary waves in finite water depth. In both Liao (2011*b*) and Xu *et al.* (2012), only a single special resonant quartet was investigated. Liu & Liao (2014) extended the work of Liao (2011*b*) from a single quartet to more complex cases, including multiple and coupled resonant quartets and resonant sextets and found that the multiple steady-state resonant waves exist in all considered cases. The existence of the multiple steady-state resonant waves was confirmed by physical experiments in a basin of the State Key Laboratory of Ocean Engineering in Shanghai (Liu *et al.* 2015). By choosing a generalized auxiliary linear operator in the HAM framework, Liao, Xu

https://doi.org/10.1017/jfm.2021.165 Published online by Cambridge University Press

& Stiassnie (2016) obtained as well steady-state nearly resonant waves in deep water and mentioned that the steady-state nearly resonant waves have nothing fundamentally different from the steady-state waves at exact resonance. Moreover, Yang, Dias & Liao (2018) obtained steady-state resonant acoustic-gravity waves in an ocean of uniform depth by means of HAM.

The steady-state resonant/near-resonant waves investigated above are all weakly nonlinear. For finite-amplitude steady-state resonant waves, Liu, Xu & Liao (2018) extended the results of Liao *et al.* (2016) from weakly nonlinear steady-state nearly resonant waves to finite-amplitude wave groups with multiple near-resonances. Liu & Xie (2019) combined the HAM-based analytical approach with a Galerkin numerical-method-based approach to obtain finite-amplitude steady-state wave groups with multiple near-resonances in finite water depth. In some cases, the numerical method can make up for the deficiencies of the analytical method, so that a fast convergent solution can be reached, as mentioned by Liu & Xie (2019). The Galerkin method was applied to SW of large amplitude and almost-limiting short-crested gravity waves in deep water by Okamura (Okamura 2003, 2010). For the nonlinear interactions between waves in a circular basin, similar numerical methods were used by Bryant (1989), which were previously applied on oblique wave groups and doubly periodic progressive permanent waves in deep water (Bryant 1984, 1985). In the present paper, we provide expressions for the steady-state second-harmonic resonant waves ((1,2)-waves) in a circular basin in which the water surface displacement η and the velocity potential φ are both represented by truncated Fourier–Bessel series. The presence of Bessel functions makes it difficult to use solely an analytical method. Therefore, following the work of Liu & Xie (2019), we combine the HAM-based analytical approach with a Galerkin numerical-method-based approach. In the HAM framework, the singularity can be avoided by only adding the resonant term in the initial guess. Then, an approximate homotopy-series solution of the HAM is used as the initial guess for the Galerkin method.

The objective of this paper is to investigate steady-state (1,2)-waves in a circular basin. The layout of the paper is as follows. The governing equations and resonance criterion are described in § 2.1. In § 2.2, we transform the original problem into a boundary-value one by using a new variable and give the solution expressions. The analytic and numerical solution procedures to obtain (1,2)-TW are explained in §§ 2.3 and 2.4, respectively. The solutions for the steady-state (1,2)-TW in a circular basin are described in § 3 and some (1,2)-wave profiles are provided with various levels of nonlinearity. The solutions for the steady-state (1,2)-SW and the procedure to obtain them are described in § 4. Conclusions and a discussion of our results are presented in § 5.

2. Mathematical framework

2.1. *Governing equations*

The classical assumptions used to derive the water-wave equations are applied. We assume that the fluid inside the circular basin is inviscid and incompressible, the flow is irrotational and surface tension is neglected. Cylindrical polar coordinates (r, θ, z) are used. The origin $(0, 0, 0)$ is at the centre of the mean horizontal free water surface, where (r, θ) lie along the mean water level and the z-axis is vertically upwards. The radius of the circular basin is R, which is chosen as the unit length. Here d denotes the ratio of depth to radius. The unit time is $(R/g)^{1/2}$, where g is the acceleration due to gravity. The governing equation is

https://doi.org/10.1017/jfm.2021.165 Published online by Cambridge University Press

Laplace's equation in cylindrical coordinates,

$$\frac{\partial^2\varphi}{\partial r^2}+\frac{1}{r}\frac{\partial\varphi}{\partial r}+\frac{1}{r^2}\frac{\partial^2\varphi}{\partial\theta^2}+\frac{\partial^2\varphi}{\partial z^2}=0,\quad r\le 1,\ -d\le z\le\eta(r,\theta,t), \tag{2.1}$$

subject to the following boundary conditions:

$$\frac{\partial\varphi}{\partial r}=0,\quad \text{on } r=1, \tag{2.2}$$

$$\frac{\partial\varphi}{\partial z}=0,\quad \text{on } z=-d, \tag{2.3}$$

$$\frac{\partial\eta}{\partial t}-\frac{\partial\varphi}{\partial z}+\frac{\partial\varphi}{\partial r}\frac{\partial\eta}{\partial r}+\frac{1}{r^2}\frac{\partial\varphi}{\partial\theta}\frac{\partial\eta}{\partial\theta}=0,\quad \text{on } z=\eta(r,\theta,t), \tag{2.4}$$

$$\frac{\partial\varphi}{\partial t}+\frac{1}{2}\left[\left(\frac{\partial\varphi}{\partial r}\right)^2+\frac{1}{r^2}\left(\frac{\partial\varphi}{\partial\theta}\right)^2+\left(\frac{\partial\varphi}{\partial z}\right)^2\right]+\eta=0,\quad \text{on } z=\eta(r,\theta,t), \tag{2.5}$$

where $\varphi(r,\theta,z,t)$ is the velocity potential and $\eta(r,\theta,t)$ the free-surface elevation. Combining the boundary conditions (2.4) and (2.5) and eliminating η gives a boundary condition only containing the velocity potential φ:

$$\frac{\partial^2\varphi}{\partial t^2}+\frac{\partial\varphi}{\partial z}+\frac{\partial\bar{f}}{\partial t}+\frac{\partial\varphi}{\partial r}\frac{\partial^2\varphi}{\partial t\partial r}+\frac{1}{r^2}\frac{\partial\varphi}{\partial\theta}\frac{\partial^2\varphi}{\partial t\partial\theta}+\frac{\partial\varphi}{\partial r}\frac{\partial\bar{f}}{\partial r}+\frac{1}{r^2}\frac{\partial\varphi}{\partial\theta}\frac{\partial\bar{f}}{\partial\theta}=0,\quad \text{on } z=\eta(r,\theta,t), \tag{2.6}$$

where

$$\bar{f}=\frac{1}{2}\left[\left(\frac{\partial\varphi}{\partial r}\right)^2+\frac{1}{r^2}\left(\frac{\partial\varphi}{\partial\theta}\right)^2+\left(\frac{\partial\varphi}{\partial z}\right)^2\right]. \tag{2.7}$$

In this section, we only consider waves rotating with angular velocity ω in the positive θ-direction. Standing waves will be considered in § 4. The linear solutions of the system (2.1)–(2.5) read

$$\bar{\eta}(r,\theta,t)=\mathrm{J}_m(k_{mn}r)\left[a\cos m(\theta-\omega t)+\alpha\sin m(\theta-\omega t)\right], \tag{2.8}$$

$$\bar{\varphi}(r,\theta,z,t)=\mathrm{J}_m(k_{mn}r)\frac{\cosh k_{mn}(z+d)}{\cosh k_{mn}d}\left[b\sin m(\theta-\omega t)+\beta\cos m(\theta-\omega t)\right], \tag{2.9}$$

where $\mathrm{J}_m(r)$ denotes the Bessel function of order m and k_{mn} denotes the nth zero of J'_m:

$$\mathrm{J}'_m(k_{mn})=0\quad (m=0,1,2,\ldots,\ n=1,2,\ldots). \tag{2.10}$$

Note that $a=m\omega b$ and $\alpha=-m\omega\beta$ since $\bar{\eta}=-\partial\bar{\varphi}/\partial t$. For steady-state symmetric waves, a, b are constants and α, β are equal to zero as mentioned by Bryant (1989). Here we study such symmetric steady-state waves. The linear solution satisfies the dispersion relation

$$m^2\omega^2=k_{mn}\tanh\ k_{mn}d. \tag{2.11}$$

For nonlinear waves dominated by the fundamental wave component (1,1) (i.e. $m=n=1$), the linear frequency is

$$\omega^2=k_{11}\tanh\ k_{11}d. \tag{2.12}$$

Due to nonlinear interactions, higher-order harmonic wave components can be generated. Under certain conditions, the harmonic wave component (m,n) will resonate with the

https://doi.org/10.1017/jfm.2021.165 Published online by Cambridge University Press

fundamental wave component (1, 1). Resonance occurs at depths such that there exists a k_{mn} satisfying

$$m(k_{11}\tanh k_{11}d)^{1/2} = (k_{mn}\tanh k_{mn}d)^{1/2}. \tag{2.13}$$

There exist different sets of resonant wave components associated with each one of the ratios of depth to radius, as shown in table 1. The case $m = n = 2$ corresponds to the second-harmonic resonance studied in the present paper.

2.2. *Expressions for the travelling-wave solutions*

Consider a steady-state resonant wave system in a circular basin dominated by the fundamental wave component (1,1), with σ denoting the actual wave frequency. Due to the nonlinearity, the actual wave frequency σ is slightly different from the linear frequency $\omega = \sqrt{k_{11}\tanh k_{11}d}$, and also depends on the wave amplitude. Write

$$\epsilon = \frac{\sigma}{\omega}, \tag{2.14}$$

where the value of ϵ is slightly different from 1. Then, we define the variable

$$\xi = \theta - \sigma t. \tag{2.15}$$

For steady-state waves, the actual wave frequency σ is independent of time. Using the new variable ξ, the original initial/boundary-value problem governed by (2.1)–(2.3), (2.5) and (2.6) can be transformed into a boundary-value problem. In the new coordinate system (r, ξ, z), the governing (2.1) becomes

$$\frac{\partial^2\varphi}{\partial r^2} + \frac{1}{r}\frac{\partial\varphi}{\partial r} + \frac{1}{r^2}\frac{\partial^2\varphi}{\partial\xi^2} + \frac{\partial^2\varphi}{\partial z^2} = 0, \quad r \le 1,\ -d \le z \le \eta(r,\xi), \tag{2.16}$$

subject to the boundary conditions

$$\frac{\partial\varphi}{\partial r} = 0, \quad \text{on } r = 1, \tag{2.17}$$

$$\frac{\partial\varphi}{\partial z} = 0, \quad \text{on } z = -d, \tag{2.18}$$

and the following two boundary conditions on the unknown free surface $z = \eta(r,\xi)$:

$$\begin{aligned}\mathcal{N}_1[\varphi] = {}& \sigma^2\frac{\partial^2\varphi}{\partial\xi^2} + \frac{\partial\varphi}{\partial z} - \sigma\frac{\partial f}{\partial\xi} - \sigma\frac{\partial\varphi}{\partial r}\frac{\partial^2\varphi}{\partial\xi\,\partial r} \\ & - \frac{\sigma}{r^2}\frac{\partial\varphi}{\partial\xi}\frac{\partial^2\varphi}{\partial\xi^2} + \frac{\partial\varphi}{\partial r}\frac{\partial f}{\partial r} + \frac{1}{r^2}\frac{\partial\varphi}{\partial\xi}\frac{\partial f}{\partial\xi} = 0, \quad \text{on } z = \eta(r,\xi),\end{aligned} \tag{2.19}$$

$$\mathcal{N}_2[\varphi,\eta] = \eta - \sigma\frac{\partial\varphi}{\partial\xi} + f = 0, \quad \text{on } z = \eta(r,\xi), \tag{2.20}$$

where

$$f = \frac{1}{2}\left[\left(\frac{\partial\varphi}{\partial r}\right)^2 + \frac{1}{r^2}\left(\frac{\partial\varphi}{\partial\xi}\right)^2 + \left(\frac{\partial\varphi}{\partial z}\right)^2\right], \tag{2.21}$$

and $\mathcal{N}_1$, $\mathcal{N}_2$ are the two nonlinear operators defined above.

https://doi.org/10.1017/jfm.2021.165 Published online by Cambridge University Press

For steady-state waves, there is no exchange of energy between different wave components, i.e. all physical quantities related to the waves are constant. Hence, according to the linear governing equation (2.16) and the linear boundary conditions (2.17) and (2.18), the symmetric steady-state wave elevation $\eta(r, \xi)$ and the velocity potential $\varphi(r, \xi, z)$ can be described by combinations of the linear solutions (2.8) and (2.9):

$$\eta = \sum_{m=0}^{\infty} \sum_{n=1}^{\infty} a_{mn} \mathrm{J}_m(k_{mn} r) \cos m\xi, \tag{2.22}$$

$$\varphi = \sum_{m=1}^{\infty} \sum_{n=1}^{\infty} b_{mn} \Psi_{mn}, \tag{2.23}$$

with

$$\Psi_{mn}(r, \xi, z) = \mathrm{J}_m(k_{mn} r) \frac{\cosh k_{mn}(z + d)}{\cosh k_{mn} d} \sin m\xi, \tag{2.24}$$

where a_{mn} and b_{mn} are constants to be determined later. Note that the velocity potential (2.23) satisfies the linear governing equation (2.16) and the boundary conditions (2.17) and (2.18) identically. Therefore, the unknown coefficients a_{mn} and b_{mn} are determined by the two nonlinear boundary conditions on the free surface (2.19) and (2.20).

2.3. *Analytic solution procedure*

Steady-state gravity wave systems near and at exact resonance were investigated by Liao (2011*b*), Xu *et al.* (2012), Liu & Liao (2014), Liao *et al.* (2016), Liu *et al.* (2018), and Liu & Xie (2019) using the HAM. Recently, Yang *et al.* (2018) obtained steady-state resonant acoustic-gravity waves in finite uniform depth using the HAM. Detailed mathematical derivations can be found in the above-mentioned articles. For the sake of simplicity, we just give the basic formulae here. In the HAM framework, for the unknown velocity potential φ and free-surface elevation η, we have the so-called homotopy-series solution:

$$\varphi(r, \xi, z) = \sum_{m=0}^{\infty} \varphi_m(r, \xi, z), \tag{2.25}$$

$$\eta(r, \xi) = \sum_{m=0}^{\infty} \eta_m(r, \xi). \tag{2.26}$$

The unknown term $\varphi_m(r, \xi, z)$ is governed by the high-order deformation equation (on $z = 0$):

$$\mathcal{L}[\varphi_m] = c_0 \Delta_{m-1}^{\varphi} + \chi_m S_{m-1} - \bar{S}_m, \tag{2.27}$$

and $\eta_m(r, \xi)$ is easily obtained from the other high-order deformation equation (on $z = 0$):

$$\eta_m = c_0 \Delta_{m-1}^{\eta} + \chi_m \eta_{m-1}, \tag{2.28}$$

where $\chi_1 = 0$ and $\chi_m = 1$ for $m > 1$, φ_0 is the initial guess of the velocity potential φ, $\mathcal{L}$ denotes the auxiliary linear operator that can be almost freely chosen, and c_0 is the so-called convergence-control parameter (which has no physical meaning). It is noteworthy that all the terms Δ_{m-1}^{φ}, S_{m-1}, $\bar{S}_m$, Δ_{m-1}^{η} on the right-hand side of (2.27) and (2.28) are determined by the known previous approximations η_j and $\varphi_j (j =$

https://doi.org/10.1017/jfm.2021.165 Published online by Cambridge University Press

$0, 1, 2, \ldots, m-1$), and can thus be regarded as known terms. The detailed expressions for Δ_{m-1}^{φ}, S_{m-1}, $\bar{S}_m$, and Δ_{m-1}^{η} are given in Appendix A.

In the HAM framework, we have great freedom to choose the auxiliary linear operator $\mathcal{L}$. Based on the linear part of (2.19), we define the auxiliary linear operator as

$$\mathcal{L}[\varphi] = \omega^2 \frac{\partial^2 \varphi}{\partial \xi^2} + \frac{\partial \varphi}{\partial z}, \tag{2.29}$$

with the property

$$\mathcal{L}[\Psi_{mn}(r, \xi, z)] = \lambda_{mn} \Psi_{mn}(r, \xi, z), \tag{2.30}$$

$$\mathcal{L}^{-1}[\Psi_{mn}(r, \xi, z)] = \frac{\Psi_{mn}(r, \xi, z)}{\lambda_{mn}}, \tag{2.31}$$

where

$$\lambda_{mn} = k_{mn} \tanh k_{mn} d - m^2 \omega^2 \tag{2.32}$$

is an eigenvalue of the auxiliary operator (2.30). Obviously, $\lambda_{mn} = 0$ corresponds to the wave resonance and leads to the singularity. When considering the second-harmonic resonance, with the definition of λ_{mn}, we always have two zero eigenvalues:

$$\lambda_{11} = \lambda_{22} = 0. \tag{2.33}$$

The fundamental wave component Ψ_{11} together with the second-harmonic resonant wave component Ψ_{22} are considered as homogeneous solutions to the auxiliary linear operator (2.30). The solution of the mth-order approximation $\varphi_m(r, \xi, z)$ is

$$\varphi_m = \varphi_m^*(r, \xi, z) + B_{11,m} \Psi_{11} + B_{22,m} \Psi_{22}, \tag{2.34}$$

where

$$\varphi_m^* = \mathcal{L}^{-1}\left[c_0 \Delta_{m-1}^{\varphi} + \chi_m S_{m-1} - \bar{S}_m\right] \tag{2.35}$$

is the particular solution of φ_m, and the unknown constants $B_{11,m}$ and $B_{22,m}$ are determined by avoiding the secular terms $\mathrm{J}_1(k_{11} r) \sin \xi$ and $\mathrm{J}_2(k_{22} r) \sin 2\xi$ appearing on the right-hand side of the $(m+1)$th-order deformation equation (2.27) for $\varphi_{m+1}(r, \xi, z)$ $(m = 1, 2, \ldots)$. To be more specific, we force the coefficients of $\mathrm{J}_1(k_{11} r) \sin \xi$ and $\mathrm{J}_2(k_{22} r) \sin 2\xi$ to be zero, thus obtaining two equations for the two unknown constants $B_{11,m}$ and $B_{22,m}$, from which the values of $B_{11,m}$ and $B_{22,m}$ can be determined. It should be emphasized that, when we substitute $\varphi_{m-1}, \varphi_{m-2}, \ldots, \varphi_0$, and $\eta_{m-1}, \eta_{m-2}, \ldots, \eta_0$ into the mth-order deformation equation (2.27), the right-hand side of (2.27) is not in the form of the solution expression (2.23). Fortunately, it can be transformed into the solution expression (2.23) form by the orthogonality properties of Bessel functions. Then, we have

$$\mathcal{L}[\varphi_m] = c_0 \Delta_{m-1}^{\varphi} + \chi_m S_{m-1} - \bar{S}_m = \sum_{p=1}^{N'} \sum_{q=1}^{N'} G_{pq} \mathrm{J}_p(k_{pq} r) \sin p\xi, \tag{2.36}$$

where G_{pq} depends upon the unknowns $B_{11,m-1}$ and $B_{22,m-1}$. The value of N' should be infinite theoretically, but is truncated in practice. With the property of the auxiliary linear

https://doi.org/10.1017/jfm.2021.165 Published online by Cambridge University Press

operator (2.31), the particular solution φ_m^* is written

$$\varphi_m^* = \mathcal{L}^{-1}\left[\sum_{p=1}^{N'}\sum_{q=1}^{N'} G_{pq}\mathrm{J}_p(k_{pq}r)\sin p\xi\right] = \sum_{p=1}^{N'}\sum_{q=1}^{N'}\frac{G_{pq}}{\lambda_{pq}}\Psi_{pq}. \tag{2.37}$$

When $m = 0$, we get the initial guess of the velocity potential φ:

$$\varphi_0 = B_{11,0}\Psi_{11} + B_{22,0}\Psi_{22}. \tag{2.38}$$

Substituting $\varphi_m, \varphi_{m-1}, \ldots, \varphi_0$, and $\eta_{m-1}, \eta_{m-2}, \ldots, \eta_0$ into the mth-order deformation equation (2.28) and utilizing the orthogonality properties of the Bessel functions, we can directly get η_m in the form of the solution expression (2.22). For the sake of simplicity, we select the initial solution of the free surface as $\eta_0 = 0$, which is also used by most traditional analytical methods.

2.4. *Numerical solution procedure*

In order to follow branches of solutions further by increasing the nonlinearity, we use a combination of the HAM and a numerical method. Numerical methods were used by Bryant (1989) when solving the nonlinear interactions between waves in a circular basin and applied to SW of large amplitude and almost-limiting short-crested gravity waves in deep water by Okamura (2003) and Okamura (2010), respectively. More recently, new algorithms have been developed to compute time-periodic solutions of the free-surface Euler equations with improved resolution, accuracy and robustness. Wilkening & Yu (2012) used the shooting method. They achieved robustness by posing the problem as an overdetermined nonlinear system and using either adjoint-based minimization techniques or a quadratically convergent trust-region method to minimize the objective function. They achieved efficiency by parallelizing the Jacobian computation. They delayed updates of the Jacobian until the previous Jacobian ceases to be useful. For accuracy, they used spectral collocation with optional mesh refinement in space and a high-order Runge–Kutta method in time. The reason for using such high-performance algorithms was to resolve a long-standing open question, posed by Penney & Price (1952), on whether the most extreme SW develop wave crests with sharp 90° corners each time the fluid comes to rest. Previous numerical studies reached different conclusions about the form of the limiting wave, but none were able to resolve the fine-scale oscillations that develop due to resonant effects. Qadeer & Wilkening (2019) developed a new algorithm to compute the Dirichlet–Neumann operator in a cylindrical geometry with a variable upper boundary. They used a transformed field expansion method that reduced the problem to a sequence of Poisson equations on a flat geometry. The solver applied for these subproblems made use of Zernike polynomials for the circular cross-section instead of the traditional Bessel functions, thus allowing spectral accuracy and a significant computational speed-up. Although the methods of Wilkening & Yu (2012) and Qadeer & Wilkening (2019) are state-of-the-art, we chose a more classical method because our purpose is not the same. Indeed, we are not interested in following branches of solutions all the way to their limiting configurations. Our purpose is simply to slightly extend the analytical results obtained with the HAM to finite-amplitude waves. Following the work of Liu & Xie (2019), we apply a Galerkin numerical-method-based approach to accelerate the convergence speed of the homotopy-series solutions and get convergent series solutions of the steady-state second-harmonic resonant waves in a circular basin. The tenth-order solution of the HAM

https://doi.org/10.1017/jfm.2021.165 Published online by Cambridge University Press

is used as the initial solution of the Galerkin method. In the numerical solution approach, we express the wave elevation η and the velocity potential φ with truncated series as

$$\eta = \sum_{m=0}^{N}\sum_{n=1}^{N} a_{mn}\mathrm{J}_m(k_{mn}r)\cos m\xi, \tag{2.39}$$

$$\varphi = \sum_{m=1}^{N}\sum_{n=1}^{N} b_{mn}\Psi_{mm}. \tag{2.40}$$

The total number of unknowns (a_{mn} and b_{mn}) is $N(2N+1)$. As the nonlinearity of the waves increases, the value of N is increased in order to reach convergence. Substituting (2.39) and (2.40) into (2.19) and (2.20), we obtain the independent relations

$$P_{i,j} = \int_0^{2\pi}\int_0^1 \mathcal{N}_1[\varphi(r,\xi,z)]r\mathrm{J}_i(k_{ij}r)\sin i\xi\,\mathrm{d}r\,\mathrm{d}\xi = 0, \quad \text{on } z=\eta(r,\xi), \tag{2.41}$$

$$Q_{i,j} = \int_0^{2\pi}\int_0^1 \mathcal{N}_2[\varphi(r,\xi,z),\eta(r,\xi)]r\mathrm{J}_i(k_{ij}r)\cos i\xi\,\mathrm{d}r\,\mathrm{d}\xi = 0, \quad \text{on } z=\eta(r,\xi). \tag{2.42}$$

The number of functionals $P_{i,j}$, $Q_{i,j}$ is the same as the number of unknown coefficients a_{mn}, b_{mn}. For given values of ϵ and d, we substitute the initial solution into (2.19) and (2.20) over a network of points in r and ξ. The initial discrete free-surface profile is

$$z=\eta(r,\xi)=\eta\left(10^{-7}+\frac{(i-1)(1-10^{-7})}{M},\frac{2\pi(j-1)}{M}\right), \quad i,j=1,2,\ldots,M+1. \tag{2.43}$$

Since r appears in the denominator of (2.19) and (2.20), we do not select discrete points at $r=0$ to avoid singularities. Note that when we choose the smallest value of r as 10^{-7} or 10^{-8}, we get the same result. Here $P_{i,j}$ and $Q_{i,j}$ and their derivatives with respect to the unknown variables are obtained by using the trapezoidal rule. Newton's iteration is used to improve the approximate homotopy-series solution. Detailed expressions of the Jacobian matrices, which are necessary for Newton's method, are shown in Appendix B. We stop the iteration if the maximum difference between the unknowns before and after the iteration is smaller than 10^{-6}.

We define the wave amplitude H as

$$H=\frac{\max[\eta(r,\xi)]-\min[\eta(r,\xi)]}{2}. \tag{2.44}$$

Table 2 shows the wave amplitude H and the absolute value of the coefficient $a_{2,2}$ for various values of N and M for $d=0.831377$ when $\epsilon=0.9989$. For different truncation numbers N ranging from 6 to 16, the values of H and $|a_{2,2}|$ remain unchanged for $M\geq 100$. Besides, the values of H and $|a_{2,2}|$ converge as N increases from 6 to 16. The truncation number N and the number of discrete points M are selected to ensure that the unknowns a_{mn} and b_{mn} are correct within three significant digits. From a purely mathematical point of view, using only three significant digits is relatively poor. But as stated above our purpose is simply to extend the branches of solutions to finite amplitude and not to get their fine details. Bessel functions are notoriously unwieldy and not suited for fast convergence (see Qadeer & Wilkening 2019). The truncation number N of the wave elevation η and velocity potential φ is given in table 3 for cases with different values of ϵ . As the

https://doi.org/10.1017/jfm.2021.165 Published online by Cambridge University Press

$N\backslash M$	60	80	100
6	(0.05165, 0.05306)	(0.05167, 0.05306)	(0.05168, 0.05306)
9	(0.05145, 0.05285)	(0.05147, 0.05286)	(0.05148, 0.05286)
12	(0.05130, 0.05260)	(0.05132, 0.05260)	(0.05133, 0.05261)
14	(0.05150, 0.05273)	(0.05150, 0.05274)	(0.05150, 0.05274)
15	(0.05153, 0.05268)	(0.05155, 0.05269)	(0.05155, 0.05269)
16	(0.05153, 0.05266)	(0.05155, 0.05266)	(0.05155, 0.05267)

Table 2. The wave amplitude H and the absolute value of the coefficient $a_{2,2}$ for various values of N and M for $d = 0.831377$ and $\epsilon = 0.9989$.

ϵ	N (Total components)	ϵ	N (Total components)
1.00014	16(272)	0.9996	9(90)
1.00013	16(272)	0.9995	9(90)
1.00012	14(210)	0.9994	9(90)
1.00011	9(90)	0.9993	12(156)
1.00010	9(90)	0.9992	12(156)
1.00008	9(90)	0.9991	14(210)
1.00005	6(42)	0.9990	14(210)
1.00001	6(42)	0.9989	16(272)
0.9999	6(42)	0.9988	16(272)
0.9998	6(42)	0.9987	16(272)
0.9997	9(90)	—	—

Table 3. Truncation number N of the wave elevation η and velocity potential φ for $d = 0.831377$ for different values of the nonlinearity ϵ.

nonlinearity increases, more terms are needed to get a convergent solution, which indicates that with increasing nonlinearity, higher-order harmonics have an increasing influence on the whole wave system. Even when $\epsilon = 0.9987$, 272 wave components are required to obtain a convergent steady-state resonant solution. Because of the difficulties associated with Bessel functions and the slow decay of coefficients (see next section), the truncation number N used in the examples shown in the present paper did not exceed 16.

3. Analysis of the results for (1,2)-TW

For TW in a circular basin, the second-harmonic resonance occurs at a ratio of depth to radius $d = 0.831377$. The corresponding resonant wave mode is the (2,2) mode. With the HAM-based analytical approach and a Galerkin numerical-method-based approach, we successfully obtained steady-state nonlinear (1,2)-TW in a circular basin. There exist convergent solutions when the dimensionless angular frequency is both slightly less than one ($\epsilon < 1$) and slightly more than one ($\epsilon > 1$). The converged results of the two branches of (1,2)-TW with different values of ϵ are listed in tables 4 and 5. If the radius of the circular basin is 1m, the water depth and the wave amplitude components in tables 4 and 5 are in metres (m). For all the steady-state resonant waves obtained in the present paper, the coefficients of the fundamental wave component (1,1) and of the second-harmonic resonant wave component (2,2) are much larger than the other wave components. This means that most of the energy of the (1,2)-wave is in the fundamental and second harmonic resonant wave components. Based on the results in the present paper, it is found that, as the

https://doi.org/10.1017/jfm.2021.165 Published online by Cambridge University Press

ϵ	$\lvert a_{1,1}\rvert$	$\lvert a_{2,2}\rvert$	$\lvert a_{3,2}\rvert$	$\lvert a_{4,3}\rvert$	$\lvert a_{1,3}\rvert$	$\lvert a_{3,4}\rvert$	H
0.9999	0.0066	0.0080	0.0002	0.0001	0.0001	—	0.0064
0.9998	0.0127	0.0145	0.0006	0.0004	0.0002	0.0001	0.0120
0.9997	0.0186	0.0202	0.0012	0.0008	0.0004	0.0003	0.0172
0.9996	0.0244	0.0253	0.0019	0.0013	0.0007	0.0005	0.0220
0.9995	0.0301	0.0300	0.0028	0.0019	0.0010	0.0007	0.0267
0.9994	0.0356	0.0343	0.0037	0.0024	0.0013	0.0011	0.0312
0.9993	0.0410	0.0384	0.0048	0.0030	0.0017	0.0015	0.0355
0.9992	0.0463	0.0422	0.0060	0.0037	0.0021	0.0019	0.0397
0.9991	0.0514	0.0459	0.0072	0.0044	0.0026	0.0025	0.0438
0.9990	0.0562	0.0493	0.0085	0.0051	0.0030	0.0031	0.0478
0.9989	0.0609	0.0527	0.0098	0.0058	0.0035	0.0038	0.0516
0.9988	0.0652	0.0559	0.0111	0.0066	0.0040	0.0045	0.0551
0.9987	0.0691	0.0590	0.0124	0.0073	0.0045	0.0054	0.0585

Table 4. Absolute values of some of the coefficients a_{mn} and wave amplitude H for $d = 0.831377$ and different values of ϵ ($\epsilon < 1$).

ϵ	$\lvert a_{1,1}\rvert$	$\lvert a_{2,2}\rvert$	$\lvert a_{3,2}\rvert$	$\lvert a_{4,3}\rvert$	$\lvert a_{1,3}\rvert$	$\lvert a_{4,2}\rvert$	H
1.00001	0.0007	0.0009	—	—	—	—	0.0007
1.00005	0.0036	0.0050	0.0001	0.0001	—	—	0.0038
1.00008	0.0060	0.0087	0.0002	0.0002	0.0001	0.0001	0.0064
1.00010	0.0078	0.0116	0.0003	0.0003	0.0001	0.0001	0.0085
1.00011	0.0087	0.0133	0.0004	0.0004	0.0001	0.0001	0.0097
1.00012	0.0098	0.0153	0.0005	0.0005	0.0002	0.0002	0.0110
1.00013	0.0110	0.0177	0.0006	0.0007	0.0002	0.0002	0.0126
1.00014	0.0126	0.0211	0.0008	0.0009	0.0003	0.0003	0.0149

Table 5. Absolute values of some of the coefficients a_{mn} and wave amplitude H for $d = 0.831377$ and different values of ϵ ($\epsilon > 1$).

nonlinearity increases (the value of $|\epsilon - 1|$ becomes larger), the amplitude of each wave component increases and so does the amplitude of the (1,2)-wave. An increasing number of higher-order harmonic wave components have non-negligible amplitudes.

Figure 1 represents $|a_{mn}|$ as a function of m or n for two values of ϵ when $\epsilon < 1$. Specifically, figures 1(a) and 1(c) show the change of the coefficient $|a_{mn}|$ as the order of the Bessel function m increases. Figures 1(b) and 1(d) show the change of $|a_{mn}|$ with the increase of the zero order n. The two points at the top left of each subplot of figure 1 represent the fundamental and second-harmonic resonant wave components, respectively. Note that $|a_{mn}|$ does not represent the magnitude of the corresponding wave component, because only the maximum amplitude of the Bessel function J_0 is 1. The maximum amplitude of $\mathrm{J}_m(m > 0)$ is less than 1 and decreases as m increases. Thus, the amplitude of the higher-order harmonic wave components is smaller than the value of $|a_{mn}|$. Therefore, as can be seen from figures 1(a) and 1(c), the amplitude of the higher-order harmonic wave components decreases as the order of the Bessel function increases. Comparing figures 1(a) and 1(b), and figures 1(c) and 1(d), it can be seen that the high-order (large n) zero terms of the low-order (small m) Bessel functions become more and more important as the nonlinearity increases. It also can be seen from figure 1 that the points representing higher-order harmonic components get closer to the two points representing the fundamental and second-harmonic resonant wave components as

https://doi.org/10.1017/jfm.2021.165 Published online by Cambridge University Press

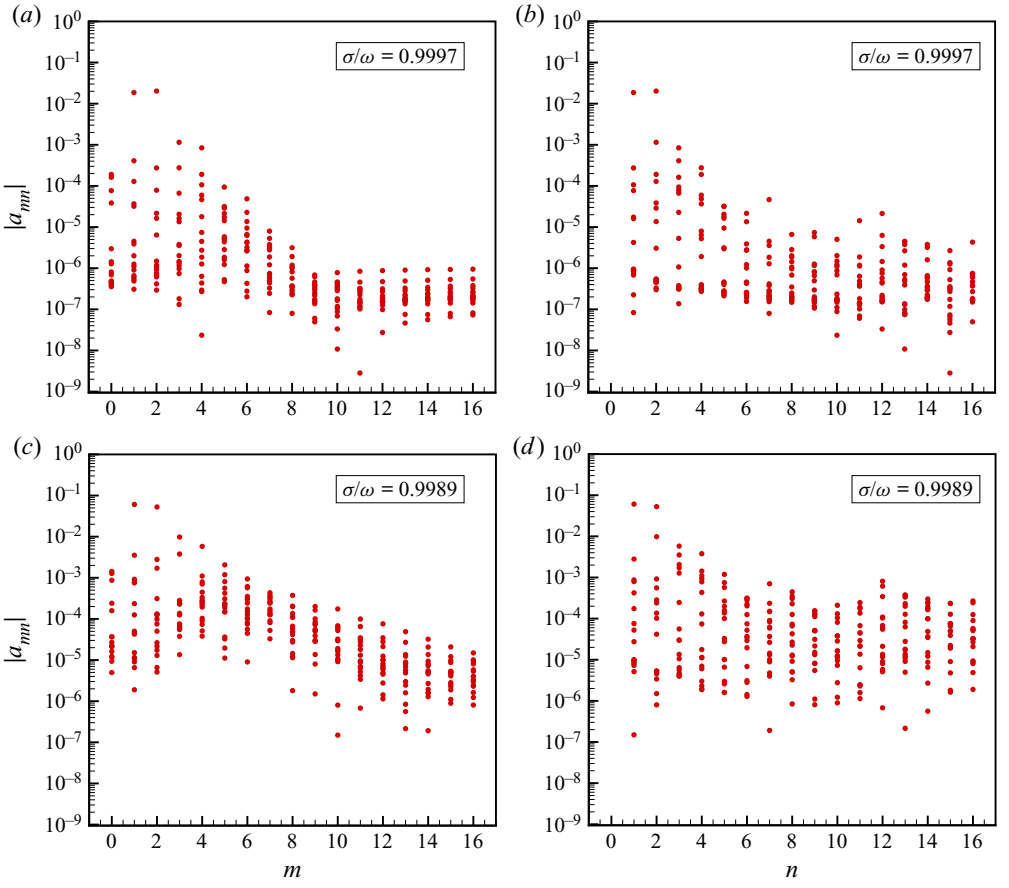

Figure 1. The absolute value of the coefficient a_{mn} as a function of m or n: (a,b) $\epsilon = 0.9997$; (c,d) $\epsilon = 0.9989$.

the nonlinearity increases. Therefore, with the growth of nonlinearity, more higher-order harmonic wave components join the (1,2)-wave.

Figure 2 shows some values of $|a_{mn}|$ as a function of ϵ. The two branches of (1,2)-TW bifurcate at $\epsilon = 1$. When $\epsilon = 1$ (infinitesimal solution), the values of a_{mn} approach 0. As $|\epsilon - 1|$ increases, $|a_{mn}|$ increases, and so does the amplitude of the (1,2)-wave. The left branch provides converged solutions with higher nonlinearity than those on the right branch. Hence, (1,2)-TW with relatively large amplitude can be obtained on the left branch. For $\epsilon < 1$, as the nonlinearity increases, the amplitude of the coefficient of the fundamental wave $|a_{11}|$ increases faster than the amplitude of the coefficient of the second-harmonic component $|a_{22}|$. However, for $\epsilon > 1$, $|a_{22}|$ increases faster than $|a_{11}|$ with increasing nonlinearity.

Figure 3 shows the ratio $|a_{22}|/|a_{11}|$ as a function of ϵ, thus demonstrating the relationship between the coefficients of the fundamental wave component and of the second-harmonic resonant wave component, and nonlinearity. Even though figure 3 represents two different branches of steady-state (1,2)-waves depending on the value of ϵ, the curves are smoothly connected. The ratio $|a_{22}|/|a_{11}|$ increases across the whole range of values of ϵ considered in the present paper. But there are some differences between the two families. When $\epsilon < 1$ and the value of $|\epsilon - 1|$ becomes large, the value of $|a_{22}|/|a_{11}|$

https://doi.org/10.1017/jfm.2021.165 Published online by Cambridge University Press

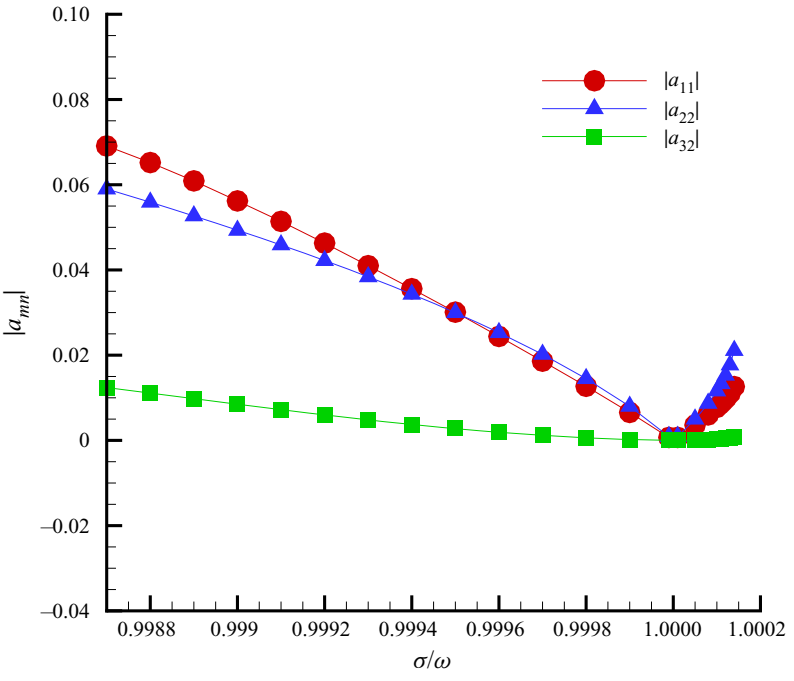

Figure 2. Some values of $|a_{mn}|$ as a function of $\epsilon = \sigma/\omega$ for (1,2)-TW.

slowly decreases. When $\epsilon > 1$ and the value of $|\epsilon - 1|$ becomes large, the trend is exactly the opposite: the curve increases sharply. The coefficient of the resonant wave component (2,2) is approximately 1.7 times the coefficient of the fundamental wave component (1,1) for the case with $\epsilon = 1.00014$. However, when $\epsilon < 1$, the coefficient of the resonant wave component (2,2) is almost the same as the coefficient of the fundamental wave component (1,1). The two branches of steady-state (1,2)-TW have different behaviours.

Away from resonance, the free surface is gently sloping and is only slightly deformed. For resonant cases, as shown in figures 4 and 5, the wave profile has two peaks in the middle, and there exists a saddle-shaped depression between the two crests (at the centre of the circular basin). This phenomenon is caused by the second-harmonic resonant wave component (2,2), which is significant for resonant cases since it has a similar amplitude to that of the fundamental wave component (1,1).

Wave profiles for (1,2)-TW with $\epsilon = 0.9997$ and $\epsilon = 0.9989$ are shown in figure 4. Here $\epsilon = 0.9997$ corresponds to a case with weak nonlinearity, while $\epsilon = 0.9989$ corresponds to a case with a stronger nonlinearity. When $\epsilon = 0.9997$, the free surface of the (1,2)-TW is smooth. However, when $\epsilon = 0.9989$, there are more ripples on the surface of the wave, that are due to the influence of higher-order harmonic wave components. The profiles for (1,2)-TW with $\epsilon = 1.00014$ are shown in figure 5. The wave profiles are similar to those with $\epsilon < 1$, but there are some differences. Comparing the conditions with $\epsilon = 0.9989$ and $\epsilon = 1.00014$ at $t = 0$, one sees that the orientation of the waveforms is different. It illustrates that $\epsilon < 1$ and $\epsilon > 1$ are associated with two different (1,2)-TW. Furthermore, since the coefficient of the resonant wave component (2,2) is approximately 1.7 times the coefficient of the fundamental wave component (1,1) for the case with $\epsilon = 1.00014$, in contrast to the case with $\epsilon = 0.9989$, the second-harmonic resonant wave component

https://doi.org/10.1017/jfm.2021.165 Published online by Cambridge University Press

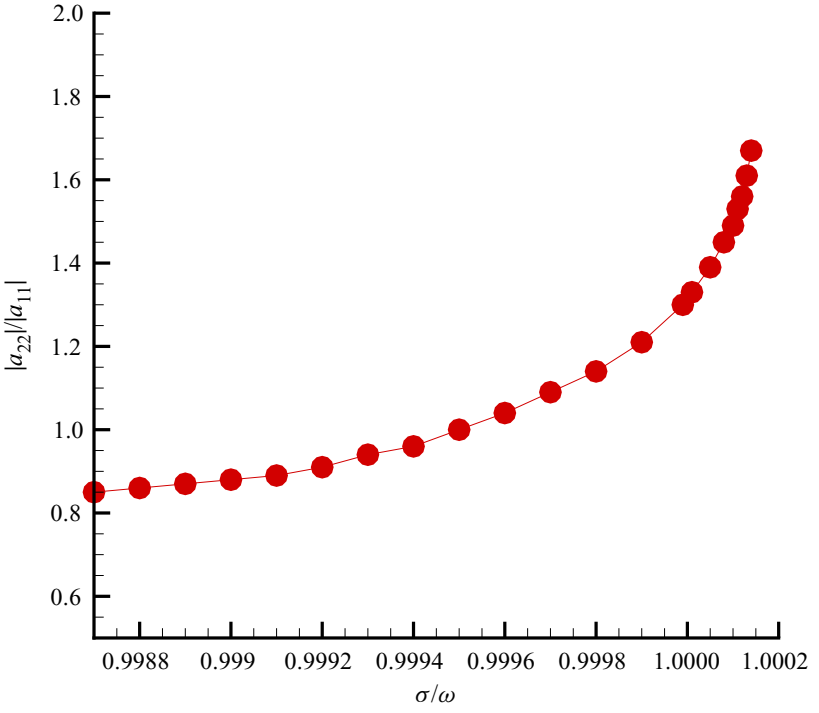

Figure 3. The value of $|a_{22}|/|a_{11}|$ as a function of $\epsilon = \sigma/\omega$ for (1,2)-TW.

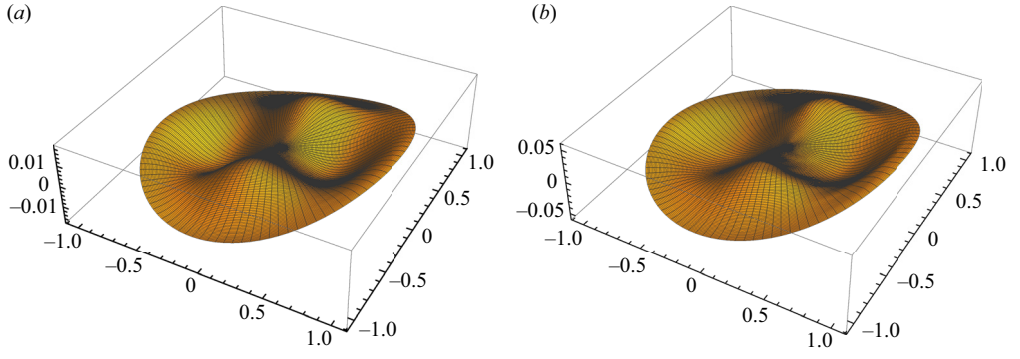

Figure 4. Wave profiles for $d = 0.831377$ at $t = 0$: (*a*) $\epsilon = 0.9997$, (*b*) $\epsilon = 0.9989$.

plays a more important role in the entire wave. The two peaks are more prominent, and the area of the two protrusions is relatively large.

4. (1,2)-SW

The same resonance can be found for SW in a circular basin. For SW, the governing equation and boundary conditions are (2.1)–(2.5) without the dependence on θ. In addition, we have the condition of mass conservation:

$$\int_0^1 r\eta_s(r, t)\,\mathrm{d}r = 0. \tag{4.1}$$

https://doi.org/10.1017/jfm.2021.165 Published online by Cambridge University Press

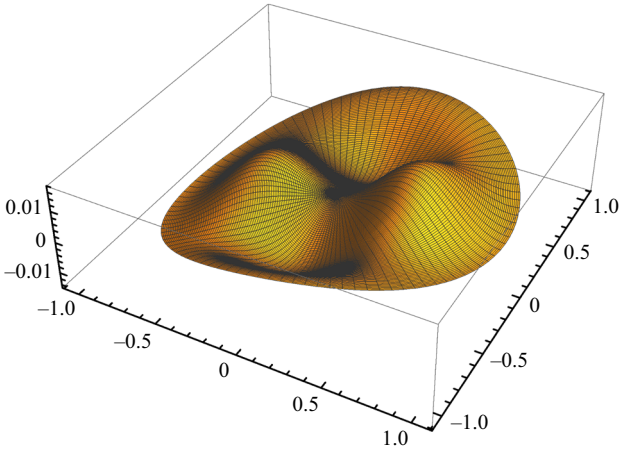

Figure 5. Wave profile for $d = 0.831377$ and $\epsilon = 1.00014$ at $t = 0$.

The linear solutions of the standing-wave system read

$$\bar{\eta}_s(r, t) = a^s \mathrm{J}_0(k_j r) \cos i(\omega_s t), \tag{4.2}$$

$$\bar{\varphi}_s(r, z, t) = b^s \mathrm{J}_0(k_j r) \frac{\cosh k_j(z + d)}{\cosh k_j d} \sin i(\omega_s t), \tag{4.3}$$

where k_j denotes the jth zero of J_0':

$$\mathrm{J}_0'(k_j) = 0 \quad (i = 1, 2, \ldots, \ j = 1, 2, \ldots). \tag{4.4}$$

The linear solution satisfies the dispersion relation

$$i^2 \omega_s^2 = k_j \tanh \ k_j d. \tag{4.5}$$

For nonlinear waves dominated by the fundamental wave component (1,1) (i.e. $i = j = 1$), the linear frequency is

$$\omega_s^2 = k_1 \tanh k_1 d. \tag{4.6}$$

Due to nonlinear interactions, higher-order harmonic wave components can be generated. Under certain conditions, the harmonic wave component (i, j) will resonate with the fundamental wave component (1, 1). Resonance occurs at ratios of depth to radius d such that there exists a k_j satisfying

$$i(k_1 \tanh k_1 d)^{1/2} = (k_j \tanh k_j d)^{1/2}. \tag{4.7}$$

There exist different sets of resonant wave components associated with each one of the ratios of depth to radius, as shown in table 6. The case $i = 2, j = 3$ corresponds to the second-harmonic resonance studied in the present paper.

Similarly, due to the nonlinearity, the actual wave frequency σ_s is slightly different from the linear frequency $\omega_s = \sqrt{k_1 \tanh k_1 d}$, and also depends on the wave amplitude. Let $\epsilon_s = \sigma_s / \omega_s$. Then, we define the variable

$$\xi_s = \sigma_s t. \tag{4.8}$$

Like for TW, we solve the standing-wave problem in a new coordinate system (r, z, ξ_s). The standing-wave elevation $\eta(r, \xi_s)$ and the velocity potential $\varphi(r, z, \xi_s)$ can be described

https://doi.org/10.1017/jfm.2021.165 Published online by Cambridge University Press

by combinations of the linear solution (4.2) and (4.3):

$$\eta_s = \sum_{i=0}^{\infty}\sum_{j=1}^{\infty} a_{ij}^s \mathrm{J}_0(k_j r)\cos i\xi_s, \tag{4.9}$$

$$\varphi_s = \sum_{i=1}^{\infty}\sum_{j=1}^{\infty} b_{ij}^s \Psi_{ij}^s, \tag{4.10}$$

with

$$\Psi_{ij}^s(r,\xi,z) = \mathrm{J}_0(k_j r)\frac{\cosh k_j(z+d)}{\cosh k_j d}\sin i\xi_s, \tag{4.11}$$

where a_{ij}^s and b_{ij}^s are constants to be determined later. Note that the velocity potential (4.10) satisfies the linear governing equation, the boundary conditions on $r=1$ and $r=-d$ and the wave elevation (4.9) satisfies the condition of mass conservation (4.1) identically. Therefore, the unknown coefficients a_{ij}^s and b_{ij}^s are determined by the two nonlinear boundary conditions on the free surface.

Like for TW, we have the so-called homotopy-series solutions for resonant SW in a circular basin for the unknown velocity potential φ_s and free-surface elevation η_s. They read

$$\varphi_s(r,z,\xi_s) = \sum_{m=0}^{+\infty}\varphi_m^s(r,z,\xi_s), \tag{4.12}$$

$$\eta_s(r,\xi_s) = \sum_{m=0}^{+\infty}\eta_m^s(r,\xi_s). \tag{4.13}$$

As opposed to the steady-state (1,2)-TW in a circular basin, we take the nonlinear frequency σ_s as an unknown quantity. The so-called homotopy-series solution about the nonlinear frequency σ_s is

$$\sigma_s = \sum_{m=0}^{+\infty}\sigma_m^s. \tag{4.14}$$

The calculations are similar to those for (1,2)-TW in a circular basin. It is worth noting that we choose the initial guess of the velocity potential φ_s as

$$\varphi_0^s = B_{11}^s\Psi_{11}^s + B_{23,0}^s\Psi_{23}^s, \tag{4.15}$$

where the constant B_{11}^s is given and corresponds to the primary wave. The unknown constants σ_0^s and $B_{23,0}^s$ are determined by avoiding the secular terms $\mathrm{J}_0(k_1 r)\sin\xi_s$ and $\mathrm{J}_0(k_3 r)\sin 2\xi_s$ appearing on the right-hand side of the first-order deformation equation. The rest of the calculation process is similar to that of the (1,2)-TW in a circular basin.

We consider the second-harmonic resonance of nonlinear SW dominated by the fundamental wave component (1,1) with ratios of depth to radius $d = 0.198143$. The corresponding resonant wave mode is the (2,3) mode. With the HAM-based analytical approach, we successfully obtain (1,2)-SW in a circular basin. The converged results with different values of B_{11}^s in the initial guess of the velocity potential are listed in table 7. It is found that, when resonance occurs, the amplitude of the fundamental wave component (1,1) and of the resonant wave component (2,3) are of the same order of magnitude. As

https://doi.org/10.1017/jfm.2021.165 Published online by Cambridge University Press

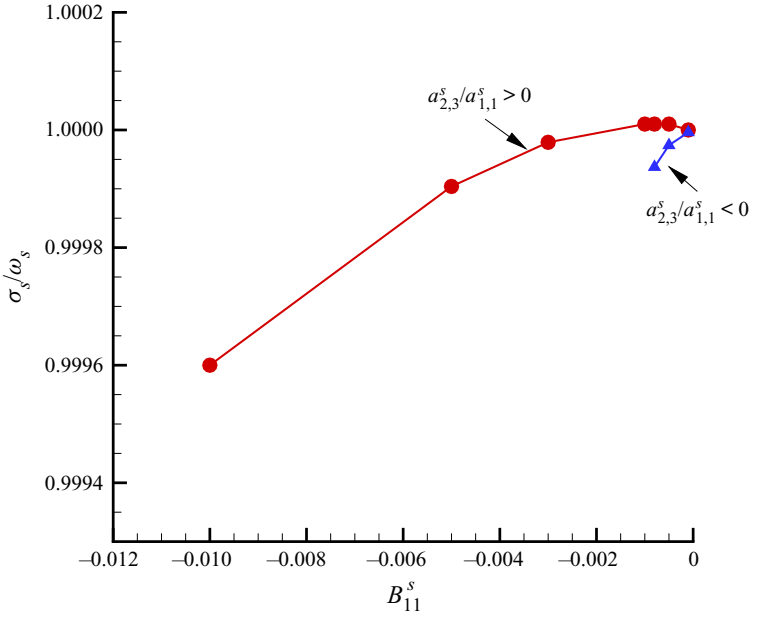

Figure 6. Value of $\epsilon_s = \sigma_s/\omega_s$ as a function of B^s_{11} for (1,2)-SW.

the value of B^s_{11} decreases, the nonlinearity of the (1,2)-SW shows an increasing trend. The amplitude coefficients in front of the fundamental wave component (1,1) and the resonant wave component (2,3) both increase. According to the variation of the value of B^s_{11}, we found two branches of convergent solutions for the (1,2)-SW in a circular basin, that correspond to the cases $a^s_{2,3}/a^s_{1,1} > 0$ and $a^s_{2,3}/a^s_{1,1} < 0$ respectively. Figure 6 shows the value of $\epsilon_s = \sigma_s/\omega_s$ as a function of B^s_{11}. The two branches of (1,2)-SW split when the value of B^s_{11} approaches 0. As the value of B^s_{11} decreases, the set of solutions $a^s_{2,3}/a^s_{1,1} > 0$ goes further.

5. Concluding remarks and discussion

The water-wave equations in a circular cylinder with nonlinear boundary conditions on the free surface are solved by a coupled analytical and numerical approach to obtain second-harmonic resonant waves with time-independent spectra. For nonlinear TW dominated by the fundamental wave component (1,1) in a circular basin, the second-harmonic wave component (2,2) resonates with the fundamental wave component (1,1) when the ratio of water depth to radius $d = 0.831377$. For nonlinear SW dominated by the fundamental wave component (1,1), the (2,3) mode resonates with the fundamental wave component (1,1) when the ratio of water depth to radius $d = 0.198143$.

In the resonance problem considered here, the second-harmonic resonant wave component corresponds to a mathematical singularity, which is difficult to deal with in the framework of perturbation methods. Additionally, the convergence rate of the series solution obtained from the HAM reduces as the nonlinearity increases. The slow convergence rate of series solutions obtained from the HAM makes it impossible to consider steady-state resonant waves with strong nonlinearity. To overcome these difficulties, a solution procedure that combines the HAM-based analytical approach and a Galerkin numerical-method-based approach has been used. Based on the HAM, when the

https://doi.org/10.1017/jfm.2021.165 Published online by Cambridge University Press

resonance occurs, only the resonant wave component needs to be added in the initial guess, and the secular term thus generated can be successfully avoided. Then, an approximate homotopy-series solution to the steady second-harmonic resonant waves can be obtained. The Galerkin numerical method-based approach is used to obtain accurate steady-state solutions. In this way, we successfully obtained steady nonlinear second-harmonic resonant waves in a circular basin. However, even the numerical method shows some slow convergence and high accuracy is difficult to reach for large nonlinearities. It will be interesting to use in future work numerical methods that do not rely on Bessel functions. The algorithm recently proposed by Qadeer & Wilkening (2019) looks promising.

This paper confirms the existence of finite-amplitude steady-state (1,2)-TW and (1,2)-SW in a circular basin. There are two branches of (1,2)-TW solutions, one with dimensionless angular frequency slightly less than one ($\epsilon < 1$) and one with dimensionless angular frequency slightly more than one ($\epsilon > 1$). The coefficients of the fundamental wave component (1,1) and of the second-harmonic resonant wave component (2,2) are much larger than the other wave components, which means that most of the wave energy resides in the fundamental and second-harmonic resonant wave components. Based on our results, the amplitude of the wave group increases continuously with the nonlinearity of the wave. As the nonlinearity increases (the value of $|\epsilon - 1|$ becomes larger), an increasing number of higher-order harmonics play a role in the whole wave. In addition, the (1,2)-resonance also exists in the case of SW in a circular basin. Similarly, there are two branches of steady-state (1,2)-SW in a circular basin.

The results in the present paper deepen our understanding of the resonance of gravity waves in a circular basin, which may occur in harbours or bays. We conclude with two suggestions for future work. Bridges (1990) showed that in addition to well-known TW and SW other classes of periodic waves, in particular three-mode MW, may exist. It will be interesting to check whether such MW can be computed with the method used in the present paper. The branches of TW and SW have different behaviours. It will be interesting to use state-of-the-art numerical methods to follow the branches towards more extreme waves.

Funding. This work was supported by the National Natural Science Foundation of China (S.J.L., grant number 11432009).

Declaration of interests. The authors report no conflict of interest.

Author ORCIDs.
Frederic Dias https://orcid.org/0000-0002-5123-4929;
Zeng Liu https://orcid.org/0000-0001-5509-9114;
Shijun Liao https://orcid.org/0000-0002-2372-9502.

Appendix A. Definitions of Δ_m^{φ}, S_m, $\bar{S}_m$ and Δ_m^{η} in (2.27) and (2.28)

The definitions of Δ_m^{φ} and Δ_m^{η} in (2.27) and (2.28) are given by

$$\Delta_m^{\varphi} = \sigma^2 \bar{\varphi}_m^{0,2} + \bar{\varphi}_{z,m}^{0,0} - 2\sigma \Gamma_{m,2} + \Lambda_m, \tag{A1}$$

$$\Delta_m^{\eta} = \eta_m - \left(\sigma \bar{\varphi}_m^{0,1} - \Gamma_{m,0}\right), \tag{A2}$$

where

$$\Lambda_m = \sum_{n=0}^{m} \left(\bar{\varphi}_n^{1,0} \Gamma_{m-n,1} + \frac{1}{r^2} \bar{\varphi}_n^{0,1} \Gamma_{m-n,2} + \bar{\varphi}_{z,n}^{0,0} \Gamma_{m-n,3} \right), \tag{A3}$$

https://doi.org/10.1017/jfm.2021.165 Published online by Cambridge University Press

with the definitions

$$\Gamma_{m,0} = \frac{1}{2}\sum_{n=0}^{m} \bar{\varphi}_n^{1,0}\bar{\varphi}_{m-n}^{1,0} + \frac{1}{2r^2}\sum_{n=0}^{m} \bar{\varphi}_n^{0,1}\bar{\varphi}_{m-n}^{0,1} + \frac{1}{2}\sum_{n=0}^{m} \bar{\varphi}_{z,n}^{0,0}\bar{\varphi}_{z,m-n}^{0,0}, \tag{A4}$$

$$\Gamma_{m,1} = \sum_{n=0}^{m}\left(\bar{\varphi}_n^{1,0}\bar{\varphi}_{m-n}^{2,0} - \frac{1}{r^3}\bar{\varphi}_n^{0,1}\bar{\varphi}_{m-n}^{0,1} + \frac{1}{r^2}\bar{\varphi}_n^{0,1}\bar{\varphi}_{m-n}^{1,1} + \bar{\varphi}_{z,n}^{0,0}\bar{\varphi}_{z,m-n}^{1,0}\right), \tag{A5}$$

$$\Gamma_{m,2} = \sum_{n=0}^{m}\left(\bar{\varphi}_n^{1,0}\bar{\varphi}_{m-n}^{1,1} + \frac{1}{r^2}\bar{\varphi}_n^{0,1}\bar{\varphi}_{m-n}^{0,2} + \bar{\varphi}_{z,n}^{0,0}\bar{\varphi}_{z,m-n}^{0,1}\right), \tag{A6}$$

$$\Gamma_{m,3} = \sum_{n=0}^{m}\left(\bar{\varphi}_n^{1,0}\bar{\varphi}_{z,m-n}^{1,0} + \frac{1}{r^2}\bar{\varphi}_n^{0,1}\bar{\varphi}_{z,m-n}^{0,1} + \bar{\varphi}_{z,n}^{0,0}\bar{\varphi}_{zz,m-n}^{0,0}\right). \tag{A7}$$

The expressions for $\bar{\varphi}_n^{i,j}$ and $\bar{\varphi}_{z,n}^{i,j}$ are

$$\bar{\varphi}_n^{i,j} = \sum_{m=0}^{n} \beta_{i,j}^{n-m,m}, \tag{A8}$$

$$\bar{\varphi}_{z,n}^{i,j} = \sum_{m=0}^{n} \gamma_{i,j}^{n-m,m}, \tag{A9}$$

with the definitions

$$\mu_{m,n} = \begin{cases} \eta_n, & m = 1, n \geq 1, \\ \displaystyle\sum_{i=m-1}^{n-1} \mu_{m-1,i}\eta_{n-i}, & m \geq 2, n \geq m, \end{cases} \tag{A10}$$

$$\psi_{i,j}^{n,m} = \frac{\partial^{i+j}}{\partial r^i \partial \xi^j}\left(\frac{1}{m!}\left.\frac{\partial \varphi_n}{\partial z^m}\right|_{z=0}\right), \tag{A11}$$

$$\beta_{i,j}^{n,m} = \begin{cases} \psi_{i,j}^{n,0}, & m = 0, \\ \displaystyle\sum_{s=1}^{m} \psi_{i,j}^{n,s}\mu_{s,m}, & m \geq 1, \end{cases} \tag{A12}$$

https://doi.org/10.1017/jfm.2021.165 Published online by Cambridge University Press

$$\gamma_{i,j}^{n,m} = \begin{cases} \psi_{i,j}^{n,1}, & m = 0, \\ \displaystyle\sum_{s=1}^{m} (s+1)\psi_{i,j}^{n,s+1}\mu_{s,m}, & m \geq 1. \end{cases} \tag{A13}$$

Due to the linear property of the auxiliary linear operator (2.29), the definitions of S_{m-1} and $\bar{S}_m$ in (2.27) are given by

$$S_m = \sum_{n=0}^{m-1} \left(\sigma^2 \beta_{0,2}^{m-n,n} + \psi_{0,0}^{m-n,n} \right), \tag{A14}$$

$$\bar{S}_m = \sum_{n=1}^{m-1} \left(\sigma^2 \beta_{0,2}^{m-n,n} + \psi_{0,0}^{m-n,n} \right). \tag{A15}$$

A similar detailed derivation for the nonlinear interaction of gravity waves in deep water can be found in the appendix of Liao (2011*b*).

Appendix B. Detailed expressions of Jacobian matrices

The elements in the Jacobian matrix are related to the derivatives of $P_{i,j}$ and $Q_{i,j}$ with respect to the unknown variables a_{mn} and b_{mn}. According to these two sets of unknowns, the Jacobian matrix can be divided into four small matrices, as shown below:

$$\frac{\partial \boldsymbol{P}_{i,j}}{\partial \boldsymbol{b}_{mn}} = \int_0^{2\pi} \int_0^1 \frac{\partial \mathcal{N}_1[\varphi]}{\partial b_{mn}} r \mathrm{J}_i(k_{ij} r) \sin i\xi \, \mathrm{d}r \, \mathrm{d}\xi, \tag{B1}$$

$$\frac{\partial \boldsymbol{Q}_{i,j}}{\partial \boldsymbol{b}_{mn}} = \int_0^{2\pi} \int_0^1 \frac{\partial \mathcal{N}_2[\varphi, \eta]}{\partial b_{mn}} r \mathrm{J}_i(k_{ij} r) \cos i\xi \, \mathrm{d}r \, \mathrm{d}\xi, \tag{B2}$$

$$\frac{\partial \boldsymbol{P}_{i,j}}{\partial \boldsymbol{a}_{mn}} = \int_0^{2\pi} \int_0^1 \frac{\partial \mathcal{N}_1[\varphi]}{\partial z} \mathrm{J}_m(k_{mn} r) \cos m\xi \cdot r \mathrm{J}_i(k_{ij} r) \sin i\xi \, \mathrm{d}r \, \mathrm{d}\xi, \tag{B3}$$

$$\frac{\partial \boldsymbol{Q}_{i,j}}{\partial \boldsymbol{a}_{mn}} = \int_0^{2\pi} \int_0^1 \frac{\partial \mathcal{N}_2[\varphi]}{\partial z} \mathrm{J}_m(k_{mn} r) \cos m\xi \cdot r \mathrm{J}_i(k_{ij} r) \cos i\xi \, \mathrm{d}r \, \mathrm{d}\xi, \tag{B4}$$

where

$$\begin{aligned} \frac{\partial \mathcal{N}_1[\varphi, \eta]}{\partial b_{mn}} = & \left[\left(-m^2\sigma^2 + \frac{2\sigma}{r^2} m^2 \varphi_\xi - \frac{m^2}{r^4} \varphi_\xi \varphi_\xi \right) \cdot \mathrm{J} \right. \\ & + \left(-2\sigma \varphi_{r\xi} + 2\varphi_r \varphi_{rr} + \frac{2}{r^2} \varphi_\xi \varphi_{r\xi} + \varphi_z \varphi_{rz} \right) \cdot \mathrm{J}_r + \varphi_r \varphi_r \cdot \mathrm{J}_{rr} \Big] \cdot CS \\ & + k_{mn} \left[\left(1 + \varphi_r \varphi_{rz} + \frac{1}{r^2} \varphi_\xi \varphi_{\xi z} - \sigma \varphi_{\xi z} \right) \cdot \mathrm{J} + \varphi_r \varphi_z \cdot \mathrm{J}_r \right] \cdot SS \\ & + 2m \left[\frac{1}{r^2} \left(-\sigma \varphi_{\xi\xi} + \varphi_r \varphi_{r\xi} + \frac{1}{r^2} \varphi_\xi \varphi_{\xi\xi} + \varphi_z \varphi_{z\xi} \right) \cdot \mathrm{J} + \left(-\sigma \varphi_r + \frac{1}{r^2} \varphi_r \varphi_\xi \right) \cdot \mathrm{J}_r \right] \cdot CC \\ & + m k_{mn} \left(-\sigma \varphi_z + \frac{1}{r^2} \varphi_\xi \varphi_z \right) \cdot \mathrm{J} \cdot SC, \end{aligned} \tag{B5}$$

$$\frac{\partial \mathcal{N}_2[\varphi, \eta]}{\partial b_{mn}} = \left(-m\sigma + \frac{m}{r^2} \varphi_\xi \right) \cdot \mathrm{J} \cdot CC + \varphi_r \cdot \mathrm{J}_r \cdot CS + k_{mn} \varphi_z \cdot \mathrm{J}_r \cdot SS, \tag{B6}$$

https://doi.org/10.1017/jfm.2021.165 Published online by Cambridge University Press

i	j	d
2	3	0.198143
2	4	0.346985
3	4	0.084425
⋮	⋮	⋮
3	10	0.439596

Table 6. Ratios of depth to radius d satisfying the linear resonance relation for standing waves (Mack 1962).

B^s_{11}	ϵ_s	$a^s_{1,1}$	$a^s_{2,3}$	H
−0.0001	1.000000	0.000157	0.000200	0.000470
	0.999996	0.000157	−0.000209	0.000041
−0.0005	1.000010	0.000783	0.000907	0.002246
	0.999974	0.000783	−0.001226	0.000430
−0.0008	1.000010	0.001253	0.001368	0.003502
	0.999937	0.001253	−0.002488	0.001306
−0.0010	1.000010	0.001567	0.001651	0.004312
−0.0030	0.999979	0.004700	0.003795	0.011695
−0.0050	0.999904	0.007834	0.005209	0.018358
−0.0100	0.999600	0.015667	0.007135	0.033649

Table 7. (1,2)-SW: dimensionless frequency ϵ_s, wave amplitude components and $H = |\eta_s(0,0) - \eta_s(1,0)|$ for $d = 0.198143$ with different values of B^s_{11} in the initial guess of the velocity potential.

$$\frac{\partial \mathcal{N}_1[\varphi,\eta]}{\partial z} = \sigma^2\varphi_{\xi\xi z}+\varphi_{zz}+\left(-2\sigma+\frac{1}{r^2}\varphi_\xi\right)\left[\left(\varphi_{rz}\varphi_{r\xi}+\varphi_r\varphi_{r\xi z}\right)+\frac{1}{r^2}\left(\varphi_{\xi z}\varphi_{\xi\xi}+\varphi_\xi\varphi_{\xi\xi z}\right)\right]$$
$$+\left(-\sigma+\frac{1}{r^2}\varphi_\xi\right)\left(\varphi_{zz}\varphi_{\xi z}+\varphi_z\varphi_{\xi zz}\right)+\varphi_{rz}\left(\varphi_r\varphi_{rr}+\frac{1}{r^2}\varphi_\xi\varphi_{\xi r}+\varphi_z\varphi_{rz}\right)$$
$$+\varphi_r\left[\left(\varphi_{rz}\varphi_{rr}+\varphi_r\varphi_{rrz}\right)+\frac{1}{r^2}\left(\varphi_{\xi z}\varphi_{\xi r}+\varphi_\xi\varphi_{r\xi z}\right)+\left(\varphi_{zz}\varphi_{rz}+\varphi_z\varphi_{rzz}\right)\right]$$
$$+\frac{1}{r^2}\varphi_{\xi z}\left(\varphi_r\varphi_{r\xi}+\frac{1}{r^2}\varphi_\xi\varphi_{\xi\xi}+\varphi_z\varphi_{\xi z}\right), \tag{B7}$$

$$\frac{\partial \mathcal{N}_2[\varphi,\eta]}{\partial z} = 1+\left(\frac{1}{r^2}\varphi_\xi-\sigma\right)\varphi_{\xi z}+\varphi_r\varphi_{rz}+\varphi_z\varphi_{zz}, \tag{B8}$$

with the definitions

$$\mathrm{J} = \mathrm{J}_m(k_{mn}r), \tag{B9}$$

$$\mathrm{J}_r = \tfrac{1}{2}k_{mn}\mathrm{J}_{m-1}(k_{mn}r) - \tfrac{1}{2}k_{mn}\mathrm{J}_{m+1}(k_{mn}r), \tag{B10}$$

$$\mathrm{J}_{rr} = \tfrac{1}{4}k^2_{mn}\mathrm{J}_{m-2}(k_{mn}r) - \tfrac{1}{2}k^2_{mn}\mathrm{J}_m(k_{mn}r) + \tfrac{1}{4}k^2_{mn}\mathrm{J}_{m+2}(k_{mn}r), \tag{B11}$$

https://doi.org/10.1017/jfm.2021.165 Published online by Cambridge University Press

and

$$CS = \frac{\cosh k_{mn}(z+d)}{\cosh k_{mn}d}\sin m\xi, \quad SS = \frac{\sinh k_{mn}(z+d)}{\cosh k_{mn}d}\sin m\xi, \tag{B12a,b}$$

$$CC = \frac{\cosh k_{mn}(z+d)}{\cosh k_{mn}d}\cos m\xi, \quad SC = \frac{\sinh k_{mn}(z+d)}{\cosh k_{mn}d}\cos m\xi. \tag{B13a,b}$$

Then, we can get the complete Jacobian matrix

$$\begin{pmatrix} \partial \boldsymbol{P}_{i,j}/\partial \boldsymbol{b}_{mn} & \partial \boldsymbol{P}_{i,j}/\partial \boldsymbol{a}_{mn} \\ \partial \boldsymbol{Q}_{i,j}/\partial \boldsymbol{b}_{mn} & \partial \boldsymbol{Q}_{i,j}/\partial \boldsymbol{a}_{mn} \end{pmatrix}. \tag{B14}$$

References

Annenkov, S.Y. & Shrira, V.I. 2006 Role of non-resonant interactions in the evolution of nonlinear random water wave fields. *J. Fluid Mech.* **561**, 181–208.

Bridges, T.J. 1990 O(2)-invariant Hamiltonians on C^4 and the (m, n) mode-interaction problem for capillary-gravity waves. *Stud. Appl. Maths* **82**, 93–120.

Bryant, P.J. 1984 Oblique wave groups in deep water. *J. Fluid Mech.* **146**, 1–20.

Bryant, P.J. 1985 Doubly periodic progressive permanent waves in deep water. *J. Fluid Mech.* **161**, 27–42.

Bryant, P.J. 1989 Nonlinear progressive free waves in a circular basin. *J. Fluid Mech.* **205**, 453–467.

Chabane, M. & Choi, W. 2019 On resonant interactions of gravity-capillary waves without energy exchange. *Stud. Appl. Maths* **142**, 528–550.

Chossat, P. & Dias, F. 1995 The 1:2 resonance with O(2) symmetry and its applications in hydrodynamics. *J. Nonlinear Sci.* **5**, 105–129.

Christodoulides, P. & Dias, F. 1994 Resonant capillary-gravity interfacial waves. *J. Fluid Mech.* **265**, 303–343.

Dias, F. & Bridges, T.J. 1990 The third-harmonic resonance for capillary-gravity waves with O(2) spatial symmetry. *Stud. Appl. Maths* **82**, 13–35.

Hammack, J.L. & Henderson, D.M. 1993 Resonant interactions among surface water waves. *Annu. Rev. Fluid Mech.* **25** (1), 55–97.

Jones, M. & Toland, J. 1985 The bifurcation and secondary bifurcation of capillary–gravity waves. *Proc. R. Soc.* A **399**, 391–417.

Kadri, U. & Akylas, T.R. 2016 On resonant triad interactions of acoustic-gravity waves. *J. Fluid Mech.* **788**, R1.

Kadri, U. & Stiassnie, M. 2013 Generation of an acoustic-gravity wave by two gravity waves, and their subsequent mutual interaction. *J. Fluid Mech.* **735**, R6.

Liao, S.J. 1992 Proposed homotopy analysis techniques for the solution of nonlinear problem. PhD thesis, Shanghai Jiao Tong University.

Liao, S.J. 2003 *Beyond Perturbation: Introduction to the Homotopy Analysis Method*. Chapman & Hall/CRC.

Liao, S.J. 2010 An optimal homotopy-analysis approach for strongly nonlinear differential equations. *Commun. Nonlinear Sci. Numer. Simul.* **15** (8), 2003–2016.

Liao, S.J. 2011*a* *Homotopy analysis Method in Nonlinear Differential Equations*. Springer.

Liao, S.J. 2011*b* On the homotopy multiple-variable method and its applications in the interactions of nonlinear gravity waves. *Commun. Nonlinear Sci. Numer. Simul.* **16** (3), 1274–1303.

Liao, S.J., Xu, D.L. & Stiassnie, M. 2016 On the steady-state nearly resonant waves. *J. Fluid Mech.* **794**, 175–199.

Liu, Z. & Liao, S.J. 2014 Steady-state resonance of multiple wave interactions in deep water. *J. Fluid Mech.* **742**, 664–700.

Liu, Z. & Xie, D. 2019 Finite-amplitude steady-state wave groups with multiple near-resonances in finite water depth. *J. Fluid Mech.* **867**, 348–373.

Liu, Z., Xu, D.L., Li, J., Peng, T., Alsaedi, A. & Liao, S.J. 2015 On the existence of steady-state resonant waves in experiments. *J. Fluid Mech.* **763**, 1–23.

Liu, Z., Xu, D.L. & Liao, S.J. 2018 Finite amplitude steady-state wave groups with multiple near resonances in deep water. *J. Fluid Mech.* **835**, 624–653.

Mack, L.R. 1962 Periodic, finite-amplitude, axisymmetric gravity waves. *J. Geophys. Res.* **67**, 829–843.

McGoldrick, L.F. 1965 Resonant interactions among capillary-gravity waves. *J. Fluid Mech.* **21**, 305–331.

Miles, J.W. 1976 Nonlinear surface waves in closed basins. *J. Fluid Mech.* **75**, 419–447.

https://doi.org/10.1017/jfm.2021.165 Published online by Cambridge University Press

MILES, J.W. 1984 Internally resonant surface waves in a circular cylinder. *J. Fluid Mech.* **149**, 1–14.
OKAMURA, M. 2003 Standing gravity waves of large amplitude in deep water. *Wave Motion* **37**, 173–182.
OKAMURA, M. 2010 Almost limiting short-crested gravity waves in deep water. *J. Fluid Mech.* **646** (7), 481–503.
PENNEY, W.G. & PRICE, A.T. 1952 Part II. Finite periodic stationary gravity waves in a perfect liquid. *Phil. Trans. R. Soc. Lond.* A **244**, 254–284.
PHILLIPS, O.M. 1960 On the dynamics of unsteady gravity waves of finite amplitude. *J. Fluid Mech.* **9** (2), 193–217.
QADEER, S. & WILKENING, J.A. 2019 Computing the Dirichlet–Neumann operator on a cylinder. *SIAM J. Numer. Anal.* **57**, 1183–1204.
VAJRAVELU, K. & VAN GORDER, R.A. 2012 *Nonlinear Flow Phenomena and Homotopy Analysis: Fluid Flow and Heat Transfer*. Springer.
VAN GORDER, R.A. & VAJRAVELU, K. 2008 Analytic and numerical solutions to the Lane–Emden equation. *Phys. Lett.* A **372** (39), 6060–6065.
VANDEN-BROECK, J.-M. 1984 Nonlinear gravity-capillary standing waves in water of arbitrary uniform depth. *J. Fluid Mech.* **139**, 97–104.
WILKENING, J. & YU, J. 2012 Overdetermined shooting methods for computing standing water waves with spectral accuracy. *Comput. Sci. Disc.* **5**, 014017.
WILTON, J.R. 1915 On ripples. *Phil. Mag. Ser. 6* **29** (173), 688–700.
XU, D.L., LIN, Z.L., LIAO, S.J. & STIASSNIE, M. 2012 On the steady-state fully resonant progressive waves in water of finite depth. *J. Fluid Mech.* **710**, 379–418.
YANG, X.Y., DIAS, F. & LIAO, S.J. 2018 On the steady-state resonant acoustic–gravity waves. *J. Fluid Mech.* **849**, 111–135.
ZHONG, X.X. & LIAO, S.J. 2017 Approximate solutions of Von Kármán plate under uniform pressure-equations in differential form. *Stud. Appl. Maths* **138** (4), 371–400.
ZHONG, X.X. & LIAO, S.J. 2018*a* Analytic approximations of Von Kármán plate under arbitrary uniform pressure-equations in integral form. *Sci. China Phys. Mech. Astronom.* **61**, 014611.
ZHONG, X.X. & LIAO, S.J. 2018*b* On the limiting Stokes wave of extreme height in arbitrary water depth. *J. Fluid Mech.* **843**, 653–679.

https://doi.org/10.1017/jfm.2021.165 Published online by Cambridge University Press